united nations
educational, scientific
and cultural
organization

international atomic
energy agency

the
abdus salam
international centre for theoretical physics

H4.SMR/1241-15

"Workshop on Three-Dimensional Modelling
of Seismic Waves Generation and their Propagation"

25 September - 6 October 2000

RECEIVER FUNCTION TECHNIQUES

Lev VINNIK

Institute of Physics of the Earth
Moscow
Russia

Receiver function techniques

Lecture notes by Lev Vinnik

Institute of Physics of the Earth, Moscow, Russia

1 Introduction

Most techniques for imaging subsurface structures, like seismic tomography, require a network of seismograph stations. Receiver functions are exceptions: they can be used with the data of a single station. The idea is to replace the network of stations by a network of seismic events. Seismic phases of body waves that are present in the seismogram can be classified into primary and secondary phases. For example, the primary P wave that arrives first is followed by secondary (reflected and converted) phases that are generated by this wave in the crust and mantl in a vicinity of the station. In order to detect the secondary phases in noise and to investigate the corresponding discontinuities, one should inspect a number of recordings of the same station. This is difficult, because source function of each event is usually different from the others, and the corresponding waveforms of secondary phases are different, as well. However, using a special kind of digital filtering (deconvolution), the primary waveform of each event can be transformed into a standard 'spike' or 'bump'. The deconvolution transforms into a standard form every secondary phase, as well, and then they can be detected by stacking the deconvolved traces with appropriate time-shift (moveout) corrections. Receiver functions and similar techniques play an important role in the present-day global and regional studies of the interior of the Earth.

2 Receiver functions in a narrow sense

The term "receiver function" was introduced for the radial component of the initial part of the seismogram $R(t)$ deconvolved by the vertical component $Z(t)$. Instead of these two components, we use L (or P) component corresponding to the principal motion direction of the P wave, and H (or SV) component, perpendicular to L in the wave propagation plane (Figure 1). $H(t)$ deconvolved by $L(t)$ can be termed receiver function, as well. Assuming that the P wave propagates in a horizontally layered isotropic medium, for every discontinuity there are three secondary phases in the H component, with comparable amplitudes (Figure 2):

Ps (converted from *P* to *S*), *Ppps* (transmitted as *P*, reflected from the free surface as *P*, and reflected from the discontinuity as *S*) and *Ppss* (transmitted as *P*, reflected from the free surface as *S* and reflected from the discontinuity as *S*). The multiple reflections of the higher order are much weaker and can be neglected. *Ps*, *Pppps* and *Ppss* are strong in the H component and missing in the L component. The only significant secondary phase in $L(t)$ is *Pppp* (*P* once reflected from the free surface and once from the discontinuity), but this phase is much weaker than the parent *P*.

2.1 Deconvolution

Deconvolution can be performed either in time or frequency domain. Frequency domain deconvolution can be performed as follows. For the L and H components, neglecting the instrument response, we can write in time domain

$$\begin{aligned} L(t) &= S(t), \\ H(t) &= S(t) * E(t), \end{aligned}$$

Where $*$ denotes convolution, $S(t)$ is source function, and $E(t)$ can be written as

$$E(t) = \alpha_1 \delta(t - \tau_1) + \alpha_2 \delta(t - \tau_2) + \ldots$$

Here α_i are amplitudes of the secondary phases, and τ_i are their delays relative to *P*. In frequency domain we can write

$$\begin{aligned} L(\omega) &= S(\omega), \\ H(\omega) &= S(\omega)E(\omega), \\ E(\omega) &= H(\omega)/L(\omega). \end{aligned}$$

Dividing the spectrum of the H component by the spectrum of the L component for extracting information on crustal structure is the essence of the spectral ratio technique, which was known prior to receiver function technique. The idea of the receiver function approach is to bring the spectral ratio in the time domain by inverse Fourier transformation. To avoid large errors caused by small values of the denominator, the spectral ratio to be Fourier transformed is modified as

$$E'(\omega) = \frac{H(\omega)\overline{L(\omega)}}{\Phi(\omega)} G(\omega),$$

where

$$\Phi(\omega) = \max\{L(\omega)\overline{L(\omega)}, c \max[L(\omega)\overline{L(\omega)}]\}.$$

The bar over L denotes the complex conjugate, and $G(\omega) = \exp(-\omega^2/4a^2)$. Constant c is called "water level" and is selected empirically. $G(\omega)$ is required to

suppress high frequencies and is also determined empirically. $E'(t)$ is recovered by inverse Fourier transformation.

The time domain deconvolution can be carried out as follows. Let the discrete representations of the actual P waveform and the desired waveform be s_k and z_k. The desired waveform is usually assumed to be δ-function: it is different from 0 only for a certain value of $k = K$.

$$\left.\begin{array}{l} s_k \text{ — seismic waveform} \\ z_k \text{ — desired waveform} \end{array}\right\} \quad k = 0, \pm 1, \pm 2, \ldots$$

If the actual P waveform is filtered with the filter l_i, the resulting waveform is

$$v_k = \sum_{i-0}^{n-1} l_i s_{k-i}.$$

We are looking for the filter, which provides minimum difference $\min Q$ between the filtered and desired waveforms

$$\begin{aligned} \varepsilon_k &= v_k - z_k, \\ Q &= \sum_k \varepsilon_k^2. \end{aligned}$$

The coefficients of this filter satisfy the condition

$$\begin{aligned} \frac{\partial Q}{\partial l_j} &= 0, \quad j = 0. \pm 1, \pm 2, \ldots, n-1, \\ \frac{\partial Q}{\partial l_i} &= 2 \sum_k \sum_{i=0}^{n-1} (l_i s_{k-i} s_{k-j} - z_k s_{k-j}). \end{aligned}$$

Here $C^s_{j-i} = \sum_k s_{k-i} s_{k-j}$ is autocorrelation of s and $R^{sz}_j = \sum_k z_k s_{k-j}$ is cross-correlation of z and s. This system can be written in the matrix form as

$$[C^s][L] = [R^{sz}].$$

Here $[L]$ is the column vector with elements l_i, $[R^{sz}]$ is the column vector with elements R_j, and $[C^s]$ is the matrix with elements C^s_{j-i}. It is assumed that the actual waveform consists of signal a and noise b

$$s_k = a_k + b_k.$$

We assume that the signal and noise are not correlated. Then matrix $[C^s]$ can be written as

$$[C^s] = \begin{bmatrix} c^a_0 + c^b_0 & c^a_1 + c^b_1 & \ldots & c^a_{n-1} + c^b_{n-1} \\ c^a_1 + c^b_1 & c^a_0 + c^b_0 & \ldots & c^a_{n-2} + c^b_{n-2} \\ \vdots & \vdots & & \vdots \\ c^a_{n-1} + c^b_{n-1} & c^a_{n-2} + c^b_{n-2} & \ldots & c^a_0 + c^b_0 \end{bmatrix}$$

The elements of this matrix are autocorrelations of a and b. In practice, the noise is assumed to be white, which means that its autocorrelation differs from 0 only for diagonal elements of the matrix. The presence of noise is accounted for by presenting the diagonal elements in the form $c_0(1 + \lambda)$. The choice of this parameter, like waterlevel parameter, is arbitrary. When it is close to 0, the resulting "spike" is very sharp, but the inversion is unstable. When λ is large (say, 100), the deconvolved waveform is close to the autocorrelation function of the actual waveform. The optimum values are in the intermediate range. The deconvolution filter transforms the actual P waveform into "spike" or "bump". In first approximation the transformed P waveforms are similar for different seismic events, and the same is true with respect to the waveforms of various secondary phases.

Instead of deconvolving every record separately, one can find a multichannel deconvolution filter for the set of records of many events. Single-channel deconvolution for continuous functions of time can be expressed as

$$v(t) = \int_{-\infty}^{+\infty} s(\tau) l(t - \tau)\, d\tau,$$

where $s(\tau)$ is the actual waveform, $l(\tau)$ is the deconvolution filter, $v(t)$ is close to the desired waveform. Multichannel deconvolution for N records is expressed as

$$v(t) = \sum_{i=0}^{N-1} \int_{-\infty}^{+\infty} s_i(\tau) l_i(t - \tau)\, d\tau.$$

In case of multichannel deconvolution, the filter for each record should be found by considering the other records. The calculations of multichannel deconvolution filter are in principle similar to the single-channel case, but require more algebra. The elements of $[C]$, $[L]$ and $[R]$ for multichannel deconvolution are matrices.

Figure 3 shows an example of multichannel deconvolution. In the left column there are three waveforms and their amplitude spectra. The dominant frequencies of the waveforms are strongly different. The results of single-channel and multichannel deconvolution of these waveforms with the same damping are shown in the middle and right column, respectively. The resulting "spike" in case of multichannel deconvolution is much sharper than in single-channel case. Multichannel deconvolution is superior to single-channel deconvolution if the amplitude spectra of the input waveforms are strongly different, like in the example in Figure 3.

2.2 Stacking receiver functions with moveout corrections

To detect weak converted and reflected phases that are present in the receiver functions, one should stack receiver functions for many events. The delay of the

converted phase relative to the parent P wave is given by

$$t(Ps) = \int_{r_d}^{r_0} \left(\sqrt{v_s^{-2} - p^2 r^{-2}} - \sqrt{v_p^{-2} - p^2 r^{-2}} \right) dr,$$

where p is ray parameter, r is the radial distance of the discontinuity, r_0 and r_d correspond to free surface and depth of conversion, v_p and v_s are P and S velocities. The time of the converted phase (its delay relative to P) is increasing with the increasing ray parameter value (or decreasing epicentral distance). For 660 km discontinuity, the difference at epicentral distances around 30 and 90 degrees is close to 10 s. To detect the converted phase, the receiver functions should be stacked with moveout travel time corrections, which depend on the ray parameter (or epicentral distance) of event and the depth of the discontinuity. In practice the stack is calculated for many assumed depths of conversion. The real signals (the converted phases) are focused at depths, which are close to depths inferred from the travel times of these phases.

Contrary to the converted phases, multiply reflected phases have an opposite dependence of travel time on the ray parameter: the delay relative to P is increasing with increasing epicentral distance. In principle, for detecting the multiples one should calculate their theoretical delays and to introduce the moveout corrections in the same way, as it was made for the converted phases. Instead, one can apply slant stacking. The moveout corrections are calculated as a differential slowness (relative to P) multiplied by differential distance. This kind of stacking implies that the delay of the signal relative to P depends linearly on epicentral distance. Strictly speaking, this is not correct, but can be used as a first approximation. Then the converted and the multiply reflected phases can be detected in the negative and positive differential slowness range, respectively. Since slowness is proportional to wavenumber, stacking the receiver functions is very similar to the conventional wavenumber-frequency filtering with the receiver array. The properties of the wavenumber filter are determined by the distribution of the seismic events with epicentral distance in about the same way, as the performance of a receiver array depends on the array aperture. If the events are concentrated in a narrow distance range, this implies filtering with a poor resolution.

Figure 4 shows the results of both kinds of stacking for a few seismograph stations. In the left column the receiver functions are stacked with moveout corrections for converted phases which are formed in the depth range between 0 and 800 km. In the right column, the same receiver functions are stacked for differential slowness between -0.30 and 0.30 s/deg. The data for station YAK contain the phases converted from the Moho (at about 5 s) and from discontinuities at about 410 km and 660 km. Time interval between 5 and 30 s is dominated by crustal multiples. The data for station SCZ in addition contain strong multiples, which arrive at about 50 s. In the data of station PAS, the multiples are dominant in the whole time window of interest. Differential slowness is the most impor-

tant (if not the only) criterion for discriminating between the signals (converted phases) and noise.

While the receiver function technique was developed for a single station, it can also be applied to seismic arrays. In that case, the receiver functions can be stacked not for separate stations, but for separate conversion points. This kind of imaging has much in common with migration in seismic exploration.

Signal/noise ratio enhancement by stacking depends on the degree of correlation between the signals in the individual traces. The effect of scatter in the traveltimes is quantified with the expression:

$$E/E_0 = 1/n + [(n-1)/n]\exp(-\sigma^2\omega^2),$$

where E is the actual energy in the stack, E_0 is the maximum possible energy, n is the number of stacked traces, ω is angular frequency of the signal, and σ is the rms value of the traveltime fluctuations. There are examples of detection of phases with a frequency of 1 Hz. Such observations are only possible if σ is not much larger than 0.1 s.

While stacking of the receiver functions is essentially a linear procedure, there are nonlinear detection techniques, like n-th root method. Instead of the initial trace, the N-th root of it with the sign preserved is taken, and the transformed traces are stacked:

$$E_N(t) = \frac{1}{M}\sum_{i=1}^{M} |l_i(t)|^{1/N} \operatorname{sign}\{l_i(t)\}.$$

The stack is raised to the N-th power, with the sign preserved

$$E'_N(t) = |E_N(t)|^N \operatorname{sign}\{E_N(t)\}.$$

There are examples when this method or equivalent techniques were used for stacking the receiver functions, but, generally, the benefits of this are not evident. First, this method distorts waveforms, and since it has no strong theoretical background, the magnitude of distortion is hard to estimate. And second, like other nonlinear techniques, it suppresses weak signals and enhances strong ones. The interest of the seismologist is usually opposite.

2.3 Inverse problem for receiver function

The secondary phases, which are present in receiver function, have different sensitivities to the properties of subsurface structure. Multiply reflected phases are sensitive to both velocity and density contrasts at the discontinuities. If the width of the discontinuity exceeds quarter of the wavelength, the reflection coefficient becomes very small. The converted phases are strongly sensitive practically only to the S velocity contrast. The transmission coefficient of the converted phase is

reduced significantly relative to the maximum value, if the width of the discontinuity is around the S wavelength or larger.

Inverse problem for receiver functions was approached in several studies dealing with crustal structures. The best way of inverting receiver functions for crustal structure would be to separate and investigate all secondary (reflected and converted) phases. This, however, is usually difficult, because they interfere with each other, and their differences in slowness are small. Therefore, generally, the wavefield should be interpreted without separating the constituent phases. Meaningful results can be obtained for plane-layered models. At high frequencies (around 1 Hz), the wavefield is dominated by scattered rather than reflected and converted phases, and the technique is applicable starting from about 0.5 Hz. Stacking the receiver functions is necessary in order to suppress scattered waves and other random features of the wavefield. In the algorithm developed in the IPE (Moscow), the synthetic SV component is calculated by using the expression

$$SV_{\mathrm{syn}}(t, v(d), c) = \frac{1}{2\pi} \int_{-\infty}^{+\infty} \frac{H_{SV}(\omega, v(d), c)}{H_L(\omega, v(d), c)} L(\omega) \exp(i\omega t)\, d\omega,$$

where $v(d)$ is a vector of the variable model parameters, c is the apparent velocity, $H_{SV}(\omega, v(d), c)$ and $H_L(\omega, v(d), c)$ are the SV and L components of the theoretical frequency response of the layered structure, and $L(\omega)$ is the spectrum of the stack of deconvolved L components. The theoretical response is computed using Thomson-Haskell matrix method. To test the model, the synthetic SV component is compared with the stack of the receiver functions. The inversion procedure is based on the general method of solving ill-posed inverse problems. The optimum parameters of the model can be found by iterative minimization of the smoothing functional:

$$F(v(d), c) = \|SV_{\mathrm{obs}}(t) - SV_{\mathrm{syn}}(t, v(d), c)\| + \alpha q(d) \|v(d) - v_0(d)\|,$$

where $v_0(d)$ is the starting velocity model, $q(d)$ is the weight functions and α is the damping parameter. The parameter α changes during the inversion procedure as $\alpha_{p+1} = \alpha_p \Delta\alpha$, where α_p is the value of α in the preceding iteration, and $\Delta\alpha$ is less than 1.0. The second term of this expression keeps the solution near the starting model. Usually the result depends on the starting model, and in order to find robust features of the solution, many experiments with different starting models are required.

The highest accuracy of the inversion is achieved in the high gradient zones, because these zones produce the converted phases, and the solution appears to be well constrained. Therefore, the best results are usually obtained for the upper and the lower crust, but not for the middle crust with a nearly constant velocity. There is a trade-off between the average velocity above the discontinuity and its depth. Using receiver functions in a broad range of epicentral distance can decrease the uncertainty.

3 Other kinds of receiver functions

There are other seismic techniques with a very similar approach to the data treatment. For example, studies of the mantle discontinuities, which are based on observations of precursors to SS, use a similar technique. Teleseismic SS phase (S wave reflected from the Earth's surface in the midpoint between the source and the receiver) is preceded by weak phases (precursors), which are reflected (or scattered) from the underside of the mantle discontinuities. In this case the parent phase is SS, and SH component of the record is deconvolved by the SH component of SS. The deconvolved records of many events at many stations with the bouncing points within certain regions are stacked. The times of the precursors relative to SS depend on the S velocity in the mantle and depths of the discontinuities. With this technique, the depths of the major mantle discontinuities (those at about 410 km and 660 km depths) were mapped worldwide. However, the accuracy of these estimates is disputable, and later I will compare them with the results of observations of the Ps converted phases at the same locations.

A similar approach was used in the analysis of multiple ScS reverberation. The coefficients of reflection of SH from the Earth's surface and the core-mantle boundary are close to unity, and the recordings of strong deep events contain a sequence of clearly visible waves reflected a few times from the free surface and the core-mantle boundary. Weaker phases, reflected from the mantle discontinuities accompany these strong ones. To detect the phases reflected from the mantle discontinuities, recordings of many events are deconvolved by ScS and the deconvolved traces are stacked with appropriate moveout corrections.

The best data on discontinuities in subduction zones are provided by observations of phases, which are converted from S to P in the source region and arrive in the tail of the P wave. In short-period frequency range these phases sometimes are detected in array recordings of deep events. Now, the receiver function technique is extended for detecting these phases in the broadband recordings of conventional seismograph stations. The idea is to deconvolve the vertical component of the teleseismic record by the S waveform in the same record and to stack the deconvolved vertical components of many records. This technique has been recently used in the search for discontinuities in the lower mantle, and some results will be shown at the end of the lecture.

Finally, reliable detection of the Ps converted phases corresponding to the uppermost mantle is hampered by arrivals of crustal multiples (see Figure 4). A possible solution of this problem is to use phases converted from S to P rather than from P to S, because the mantle converted phases Sp arrive earlier than the crustal multiples. The appropriate technique (S receiver function technique) has been introduced recently. Examples of application of this technique will be shown later. They include analysis of structure of the upper layer of the Moon.

4 Receiver functions for anisotropic media

In the isotropic, laterally homogeneous medium the P wave is coupled only with SV. In anisotropic medium, all three components of motion (vertical Z, radial R and transverse T) are coupled.

One of the most useful techniques for measuring azimuthal anisotropy in the mantle is closely related to the receiver function technique. In azimuthally anisotropic medium, S wave with a nearly vertical direction of propagation splits into two quasi-shear waves, which propagate with different velocities, and polarizations of which are perpendicular to the wave propagation direction and to each other. Assume that on its way to the Earth's surface the S wave propagates through an anisotropic layer. Neglecting the vertical component, the relationship between the radial (R) and transverse (T) components of this wave above the layer and its SV and SH components beneath the layer can be described in frequency domain by matrix equation

$$[A(\omega)] = [F(\omega)][S(\omega)],$$

where $[A(\omega)]$ is column vector with the elements $R(\omega)$ and $T(\omega)$; $[S(\omega)]$ is column vector with elements $SV_0(\omega)$ and $SH_0(\omega)$; matrix $[F(\omega)]$ contains transfer functions

$$\begin{bmatrix} R_{SV}(\omega) & R_{SH}(\omega) \\ T_{SV}(\omega) & T_{SH}(\omega) \end{bmatrix}.$$

Approximate expressions for the transfer functions can be obtained by using Figure 5. Incoming S wave in Figure 5 is SV with the vertical incidence and unit amplitude. In anisotropic layer with a horizontal symmetry axis the incoming wave splits into the fast and slow quasi-shear waves. Polarization of the fast wave is parallel to the crystallographic axis a in olivine. Fast direction forms angle β with direction R. Arrows show amplitudes of the incoming and split waves. Amplitudes of the split waves are equal to $\cos\beta$ and $\sin\beta$ for the fast and slow split waves, respectively. Amplitudes of the transfer functions can be obtained by projecting the amplitudes of the split waves on the axes R and T. The resulting expressions for the transfer functions are

$$\begin{aligned} R_{SV}(\omega) &\approx \cos^2\beta + \sin^2\beta \exp(-i\omega\,\delta t), \\ T_{SV}(\omega) &\approx R_{SH}(\omega) \approx -0.5 \sin 2\beta[1 - \exp(-i\omega\,\delta t)], \\ T_{SH}(\omega) &\approx \sin^2\beta + cos^2\beta \exp(-i\omega\,\delta t). \end{aligned}$$

Here δt is the traveltime delay of the slow split wave relative to the fast one. Thus, the effect of azimuthal anisotropy can be described by two parameters: (1) fast direction (polarization direction of the fast split wave) and (2) delay of the slow wave relative to the fast one. First parameter is controlled by the direction of symmetry axis in the anisotropic layer. Second parameter is proportional to the

strength of anisotropy (difference between the fast and slow velocity) and the thickness of the layer.

Measurements of the parameters of anisotropy beneath the seismograph station are based on the recordings of seismic phase SKS. This phase propagates as the S wave in the mantle and as P wave in the liquid core of the Earth. Due to coupling between SV and P at the core/mantle boundary SKS in isotropic Earth should be polarized as SV. Putting $SH_0(\omega) = 0$ in the expressions for $R(\omega)$ and $T(\omega)$, we get

$$SV_0(\omega) = R(\omega)/R_{SV}(\omega)$$

and

$$T(\omega) = T_{SV}(\omega)R(\omega)/R_{SV}(\omega).$$

Using last expression we can find the theoretical $T(\omega)$ for any pair of the parameters of anisotropy and (by inverse Fourier transformation of $T(\omega)$) the related synthetic seismogram of the T component of SKS phase. The optimum pair provides minimum rms difference between the observed and synthetic T components. This approach has much in common with the receiver function inversion: in both cases one component of wave moton is used to synthesize the other component. In both cases the optimum model minimizes the difference between the observed and synthetic components.

At long periods ($\omega\,\delta t \ll 1$) the harmonic components of SKS are related as

$$R(t) \approx \cos\omega t,$$
$$T(t) \approx 0.5\omega\,\delta t \sin 2\beta \sin\omega t.$$

This means that the T component of SKS is shifted in time with respect to the R component by a quarter period, and its amplitude is proportional to frequency. In other words, the T component is proportional to the derivative of the R component. This relation between the R and T components of SKS allows to recognize the effect of azimuthal anisotropy and to distinguish it from lateral heterogeneity. The term $\sin 2\beta$ means that T/R amplitude ratio is a harmonic function of azimuth with a period of π.

These properties suggest an alternative technique for processing SKS recordings. Contribution of azimuthal anisotropy to the T component of SKS can be retrieved by deconvolving the T component of many recordings by the respective R component and stacking the deconvolved T components with weights depending on back azimuth of the event. The weight W_i is defined as

$$W_i = \cos 2(\varphi_i - \psi) \Big/ \sum_{i=1}^{n} \cos^2 2(\varphi_i - \psi),$$

where φ_i is back azimuth of the i-th event, n is the number of events, and ψ is a variable parameter. The stacking allows to isolate second azimuthal harmonic (with a period of π). The value of ψ, which provides maximum amplitude of

the stack has meaning of phase of this harmonic. This value differs from the fast direction of anisotropy by ± 45 degrees. The value of δt corresponds to the maximum amplitude of the stack.

Observations of SKS provide excellent lateral resolution but they are insensitive to depth of anisotropy. Distribution of anisotropy with depth can be constrained with the aid of receiver functions. In an isotropic laterally homogeneous Earth, secondary (converted and reflected) phases are polarized strictly in the vertical plane containing the source and the receiver, and their amplitudes are independent of the azimuth. In the presence of azimuthal anisotropy, an appreciable amount of energy of the secondary phases is contained in the T component, and the amplitude of the SV component depends on the azimuth. There are two different mechanisms responsible for the T component of the Ps phases. If this phase is converted from the boundary between two isotropic media, the T component can arise from the splitting of SV. This mechanism is exploited in the SKS techniques. If the phase is converted from the discontinuity between anisotropic media with different anisotropies or from the discontinuity between isotropic and anisotropic media, the T component, like SV, is generated directly by conversion from P. In the process of further propagation, both the SV and T component are modified by shear wave splitting.

Figure 6 demonstrates synthetic seismograms for a medium with azimuthal anisotropy. Anisotropy is hexagonal with a horizontal axis of symmetry. This is the simplest kind of anisotropy that is consistent with the properties of crust and mantle rocks. Anisotropy is in the layer between 30 and 180 km depths, fast direction of anisotropy is 0 degrees, velocities of the fast and slow split waves differ by 3%. Isotropic discontinuity is placed at a depth of 410 km. The only strong wave in the L component is P wave at a time of 0 s. It is followed by arrival at a time of 3 s, which is seen in both H and T components. This phase is formed by conversion from P to S at the upper boundary of the anisotropic layer. Two phases which arrive at a time around 10–12 s are multiple reflections (from the free surface and the upper boundary of the anisotropic layer). Tho phases that arrive at a time around 18 s are formed by conversion from P to S at the lower boundary of the anisotropic layer and by subsequent splitting of the S wave in this layer. Finally, the phases that arrive at a time ariund 40 s are formed by conversion from P to S at a depth of 410 km and splitting of S in the anisotropic layer. There are strong differences between polarities and amplitudes of differet phases in the same component and between those of the same phase in different components.

We filtered H and T components of this wavefield in azimuth domain by stacking the traces with weights W_i depending on their azimuths. The weights are different for the H and T components and are defined as

$$W_i^T(\psi) = \sin 2(\psi - \varphi_i) \Big/ \sum_{j=1}^{n} \sin^2 2(\psi - \varphi_j),$$

$$W_i^H(\psi) = -\cos 2(\psi - \varphi_i) \Big/ \sum_{j=1}^{n} \cos^2 2(\psi - \varphi_j),$$

where φ is back azimuth of the i-th trace, and ψ is a variable parameter. These filters isolate second azimuthal harmonic with a period of π and introduce a phase shift between the stacks of H and T components in azimuth domain. The results of azimuthal filtering of traces in Figure 6 are presented in Figure 7. In spite of differences between the initial H and T components, the stacked traces are remarkably similar. This similarity presents an important criterion to distinguish azimuthal anisotropy from lateral heterogeneity. The actual receiver functions in a broad range of azimuths should be stacked with the azimuth-dependent weights like synthetics in Figure 6. The results of stacking can be inverted for subsurface structure by comparing them with the synthetics that are processed like the actual recordings. The optimum model should also be consistent with the observations of SKS at the same station. Examples of processing and interpreting the actual data will be demonstrated.

Processing of the secondary phases related to the P wave can be complemented by analysis of precursors to the teleseismic S. The precursors contain waves converted from S to P in a vicinity of the station but no crustal multiples. To detect the Sp phases and their azimuthal variations caused by azimuthal anisotropy we have developed a stacking technique, which can be termed the S receiver function technique. We decompose the three-component seismogram is decomposed into P, SV and T components. SV corresponds to the principal particle motion direction in the wave propagation plane. The P axis is perpendicular to the SV axis in the same plane. Orthogonality of the SV and P axes allows to observe the Sp phases in the P component without interference with the stronger S wave. The P component of every recording is deconvolved by the principal (M) component of the S wave motion.

The deconvolved recordings are separated into groups. Back azimuths of the events of one group are close to each other, whereas their focal mechanisms are different. For each group we can derive the P component (observed at the free surface) corresponding to the incident SV in the isotropic half-space (beneath the anisotropic layers) and deconvolved by the SV observed at the free surface. This component can be obtained by stacking the deconvolved P components with weights depending on the level of noise and the angle between the M direction and backazimuth of the event. Various models can be tested by comparing this component with the corresponding synthetics. The technique was tested and allowed to detect, among other phases of interest, the Sp phase related to Lehman discontinuity at a depth of 230 km.

5 Examples of applications of the receiver function techniques

Applications of the receiver function techniques will be illustrated with results of several recent studies. The geophysical problems to be addressed are as follows:

1. Detailed structure of the upper mantle discontinuities in the Kuril-Japan subduction zone.
2. Topography of the upper mantle discontinuities on a global scale.
3. Teleseismic travel-time residuals in North America, as derived from receiver functions, and anelasticity of the asthenosphere.
4. Search for discontinuities in the lower mantle.
5. Depth dependent anisotropy in central Europe by P and S receiver functions.
6. Seismic evidence of flow at the base of the upper mantle.
7. Crustal structure of the Moon.

References

[1] Ammon, Ch.J., G.E. Randall, and G. Zandt, On the nonuniqueness of receiver function inversions, J. Geophys. Res., 95, 15303-15318, 1990.

[2] Berkhout, A.J. Least square inverse filtering and wavelet deconvolution, Geophysics, 42, 1369-1383, 1977.

[3] Cassidy, J.F., Numerical experiments in broadband receiver function analysis, Bull. Seism. Soc. Am., 67, 677-691, 1992.

[4] Chevrot, S., L. Vinnik, and J.-P. Montagner, Global scale analysis of the mantle Pds phases, J. Geophys. Res., 104, 20203-20219, 1999.

[5] Duecker, K. G., and A. F. Sheehan, Mantle discontinuity structure from midpoint stacks of converted P to S waves across the Yellowstone hotspot track, J. Geophys. Res., 102, 8313-8327, 1997.

[6] Farra, V., and L. Vinnik, Upper mantle stratification by P and S receiver functions, Geophys. J. Int., 141, 699-712, 2000.

[7] Flanagan, M., and P. Shearer, Global mapping of topography on transition zone velocity discontinuities by stacking SS precursors, J. Geophys. Res., 103, 2673-2692, 1998.

[8] Kanasevich, R. E., C.D. Hemmings, and T. Alpaslan, N-th root stack nonlinear multichannel filter, Geophysics, 38, 327-338, 1973.

[9] Karato, S., Importance of anelastcity in the interpretation of seismic tomography, Geophys. Res. Lett.,20, 1623-1626, 1993.

[10] Keith, C. M. and S. Crampin, Seismic body waves in anisotropic media: Propagation through a layer, Geophys. J. R. astr. Soc., 49, 209-223, 1977.

[11] Kosarev, G.L., L.I. Makeyeva, and L.P. Vinnik, Anisotropy of the mantle inferred from observations of P to S converted waves, Geophys. J. R. astr. Soc., 76, 209-220, 1984

[12] Kosarev, G. L., N. V. Petersen, L. P. Vinnik, and S.W. Roecker, Receiver functions for the Tien Shan analog broad-band network - contrasts in the evolution of structures across the Talasso-Fergana fault, J. Geophys. Res., 98, 4437-4448, 1993.

[13] Langston, C. A., Structure under mount Rainier, Washington, inferred from teleseismic body waves, J. Geophys. Res., 84, 4749-4762, 1979.

[14] Levin, V., and J. Park, P-SH conversions in a flat-layered medium with anisotropy of arbitrary orientation,Geophys. J. Int., 131, 253-266, 1997.

[15] Petersen, N., and L. Vinnik, Detection of crustal converted phases as a problem of multichannel filtering, Proc. Acad. Sci. Russ., Physics of the Earth, 4, 37-44, 1991 (in Russian).

[16] Revenaugh, J., and T.H. Jordan, A study of mantle layering beneath the Western Pacific, J. Geophys. Res., 94, 5787-5813, 1989.

[17] Savage, M.K., Lower crustal anisotropy or dipping boundaries? Effects on receiver functions and a case study in New Zealand, J. Geophys. Res., 103, 15069-15087, 1998.

[18] Vinnik, L.P., Detection of waves converted from P to SV in the mantle, Phys. Earth Planet. Inter., 15, 39-45, 1977.

[19] Vinnik, L.P., G.L. Kosarev, and L.I. Makeyeva, Lithospheric anisotropy as indicated by SKS and SKKS waves, Doklady - Earth Sci. Sections, 278, 39-43 (published in English by Scripta Technica), 1984.

[20] Vinnik, L.P., R. Kind, G.L. Kosarev, and L.I. Makeyeva, Azimuthal anisotropy in the lithosphere from observations of long-period S waves, Geophys. J. Int., 99, 549-559, 1989.

[21] Vinnik, L., S. Chevrot, and J.-P. Montagner, Seismic evidence of flow at the base of the upper mantle, Geophys. Res. Lett., 25, 1995-1998, 1999.

[22] Vinnik, L., S. Chevrot, J.-P. Montagner, and F. Guyot, Teleseismic travel time residuals in North America and anelasticity of the asthenosphere, Phys. Earth Planet. Inter., 116, 93-103, 1999.

[23] Vinnik, L., M. Kato, and H. Kawakatsu, Search for discontinuities in the lower mantle, Geophys. J. Int., submitted, 1999.

Figure 1

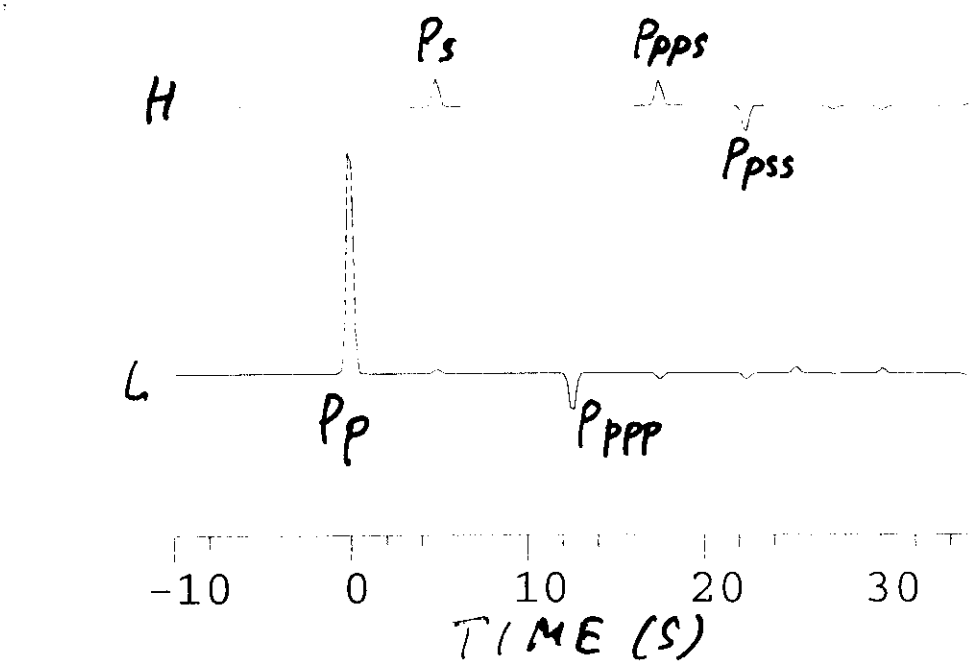
Ps
Ppps
H
Ppss
L
Pp
Pppp
-10
0
10
20
30
TIME (S)

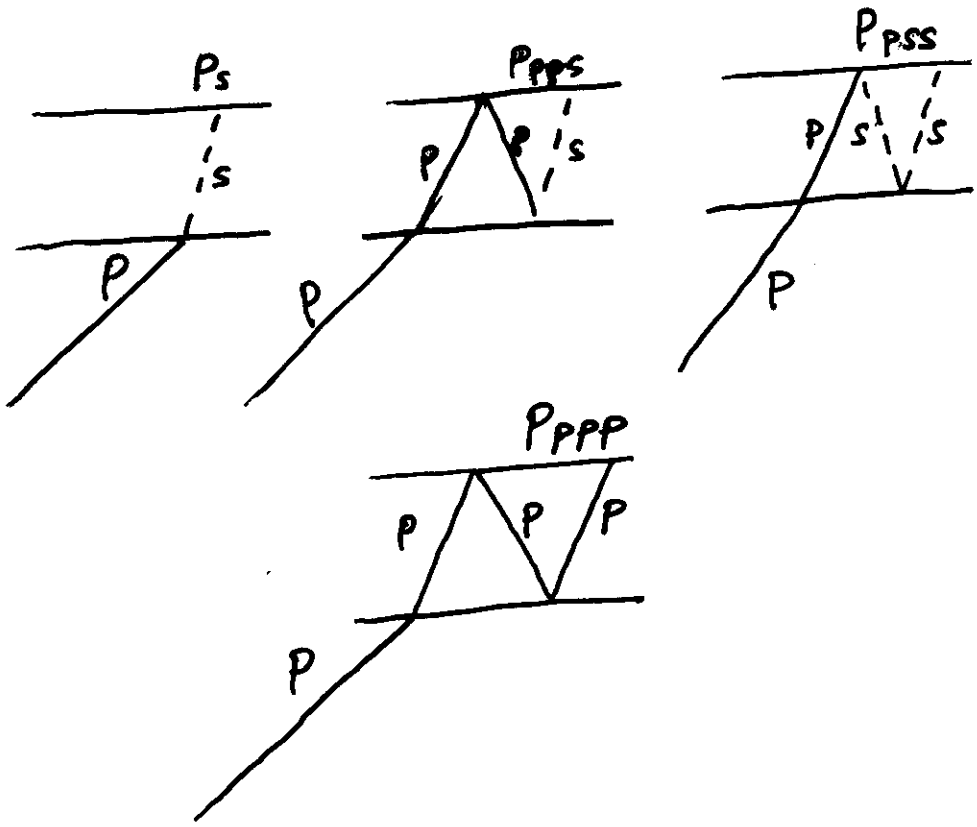
Ps
s
P
Ppps
P
P
s
P
Ppss
P
s
s
P
Pppp
P
P
P
P

Figure 2

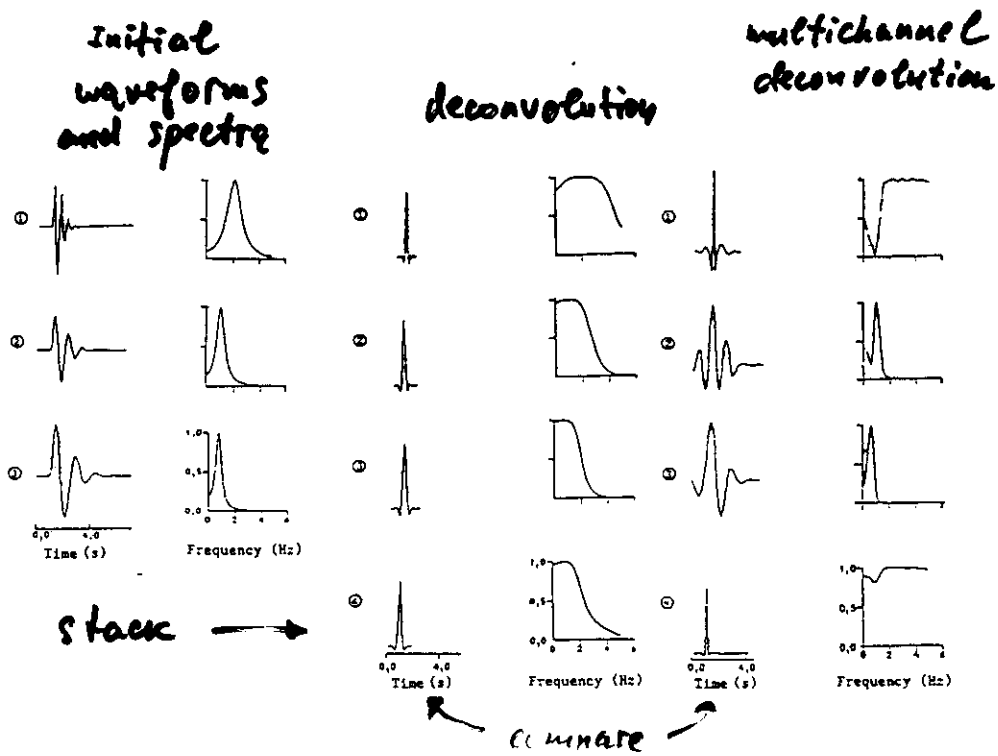
Initial waveforms and spectra
deconvolution
multichannel deconvolution
Time (s)
Frequency (Hz)
stack
Time (s)
Frequency (Hz)
Time (s)
Frequency (Hz)
Correlate

Figure 3

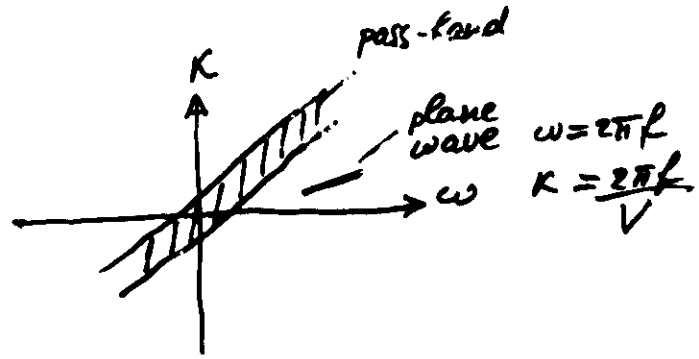
K
pass-band
plane wave
ω
ω = 2πf
K = 2πf/V

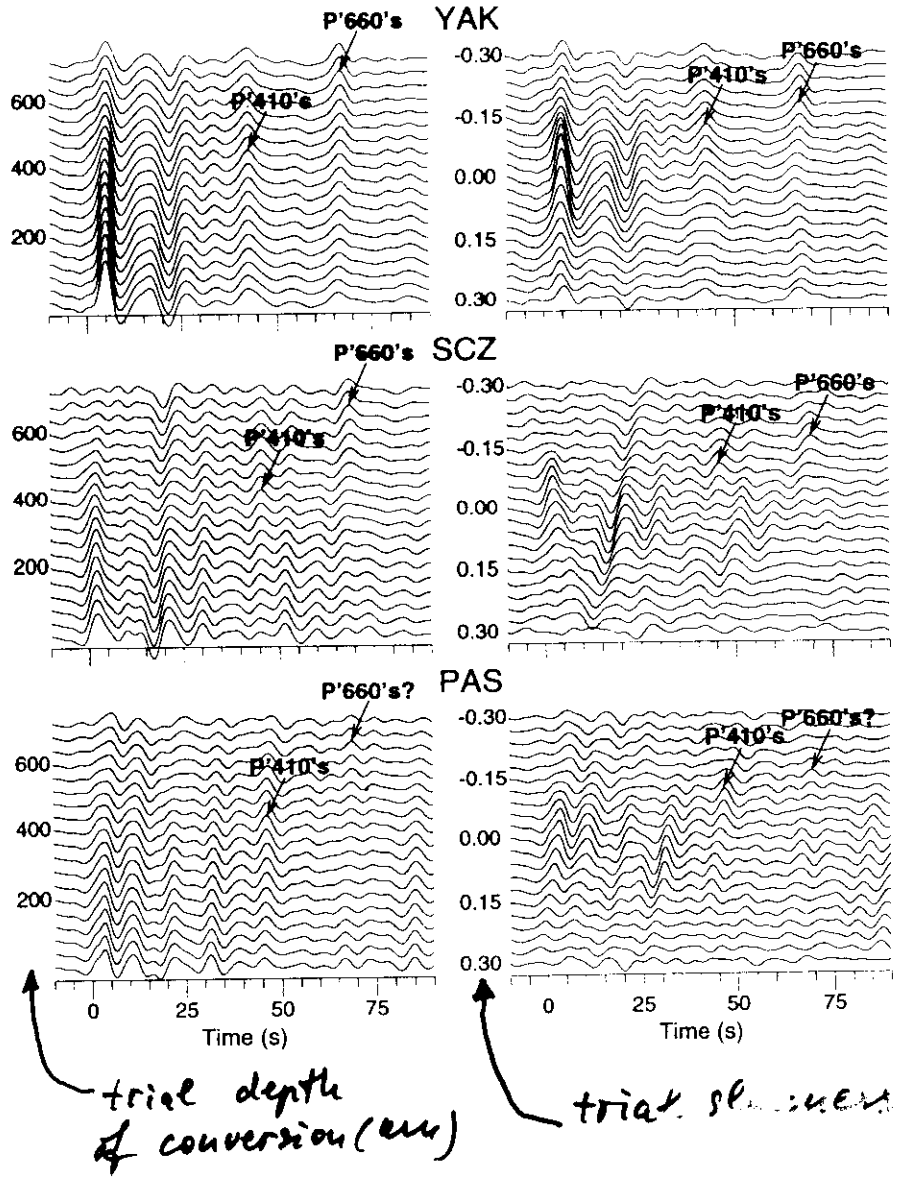
YAK
SCZ
PAS
P'660's
P'410's
P'660's?
600
400
200
-0.30
-0.15
0.00
0.15
0.30
0
25
50
75
Time (s)
trial depth of conversion (km)
trial slowness (s/deg)

Figure 4

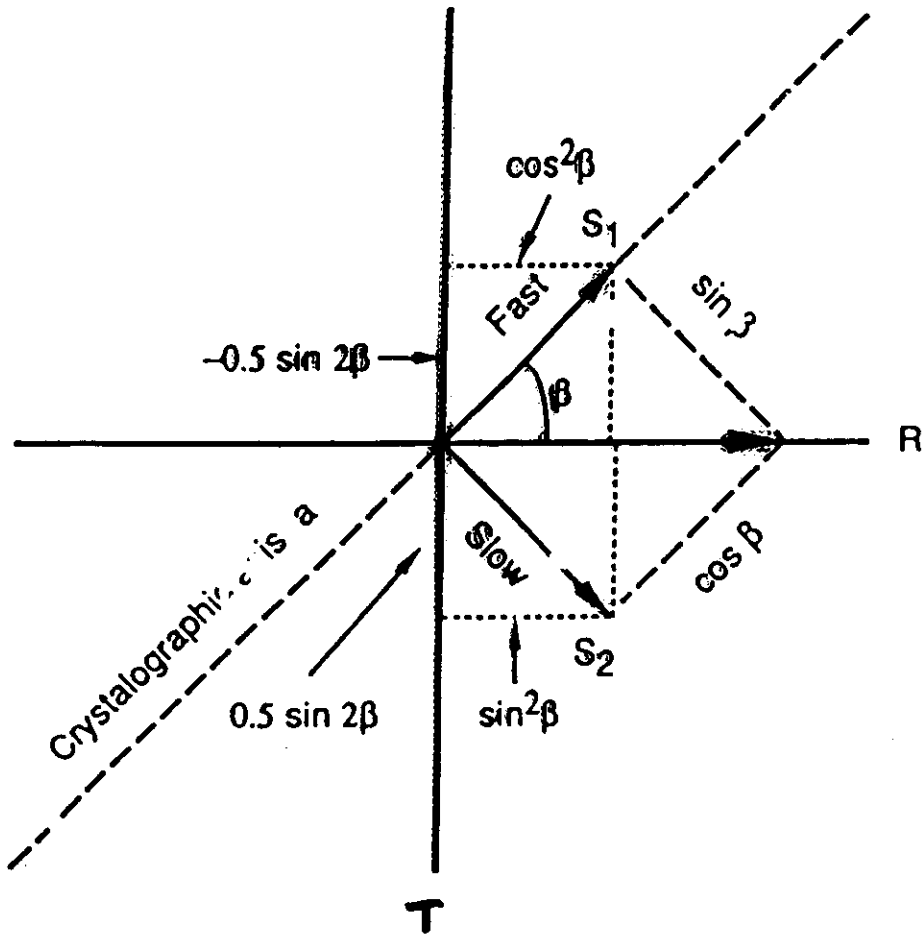
cos²β
S1
Fast
sin β
-0.5 sin 2β
β
R
Slow
cos β
S2
Crystalographic c is a
0.5 sin 2β
sin²β
T

Figure 5

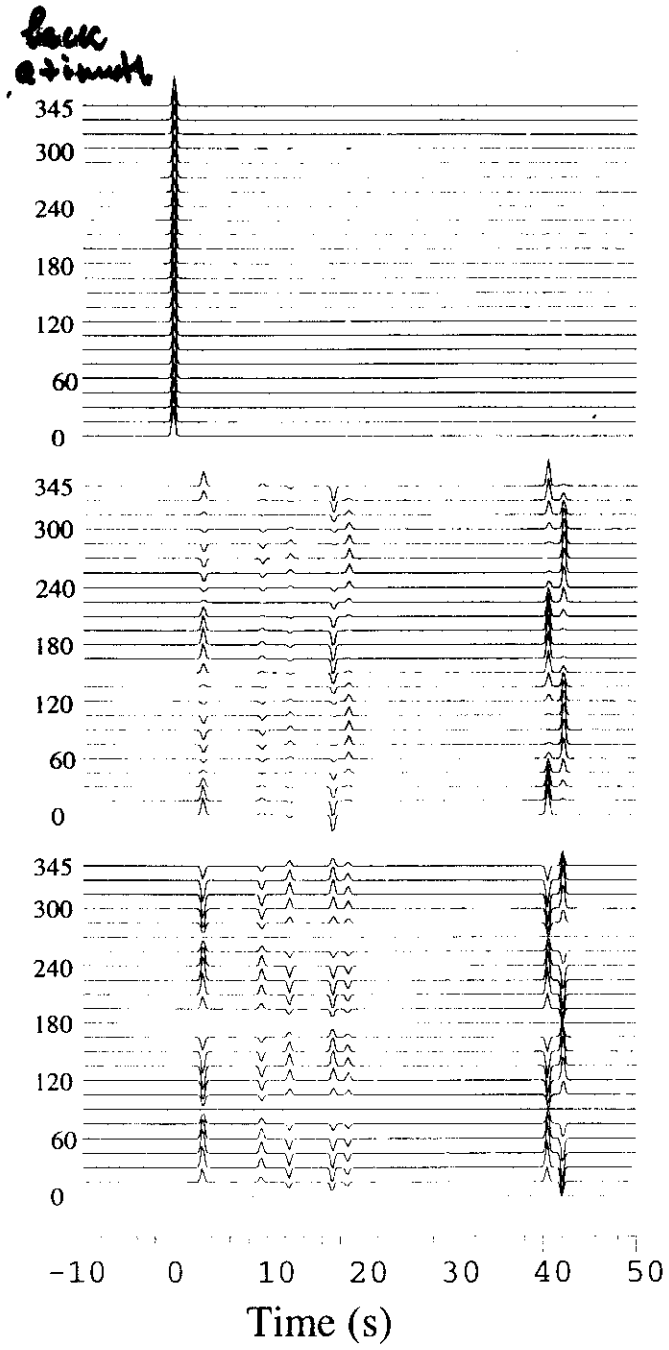
back azimuth
345
300
240
180
120
60
0
-10
0
10
20
30
40
50
Time (s)

L

H

T

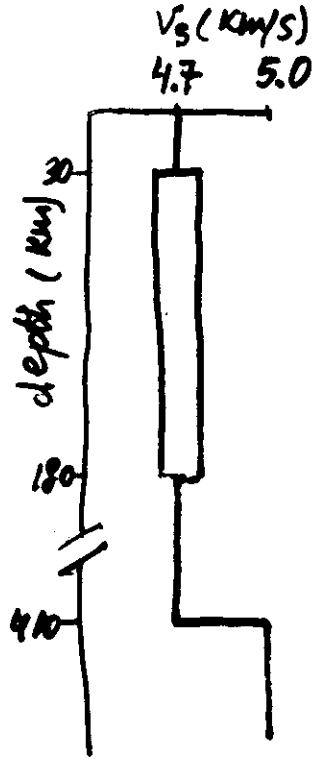
V_S (Km/s)
4.7
5.0
depth (Km)
30
180
410

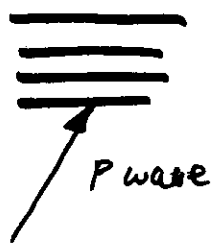
P wave

Figure 6

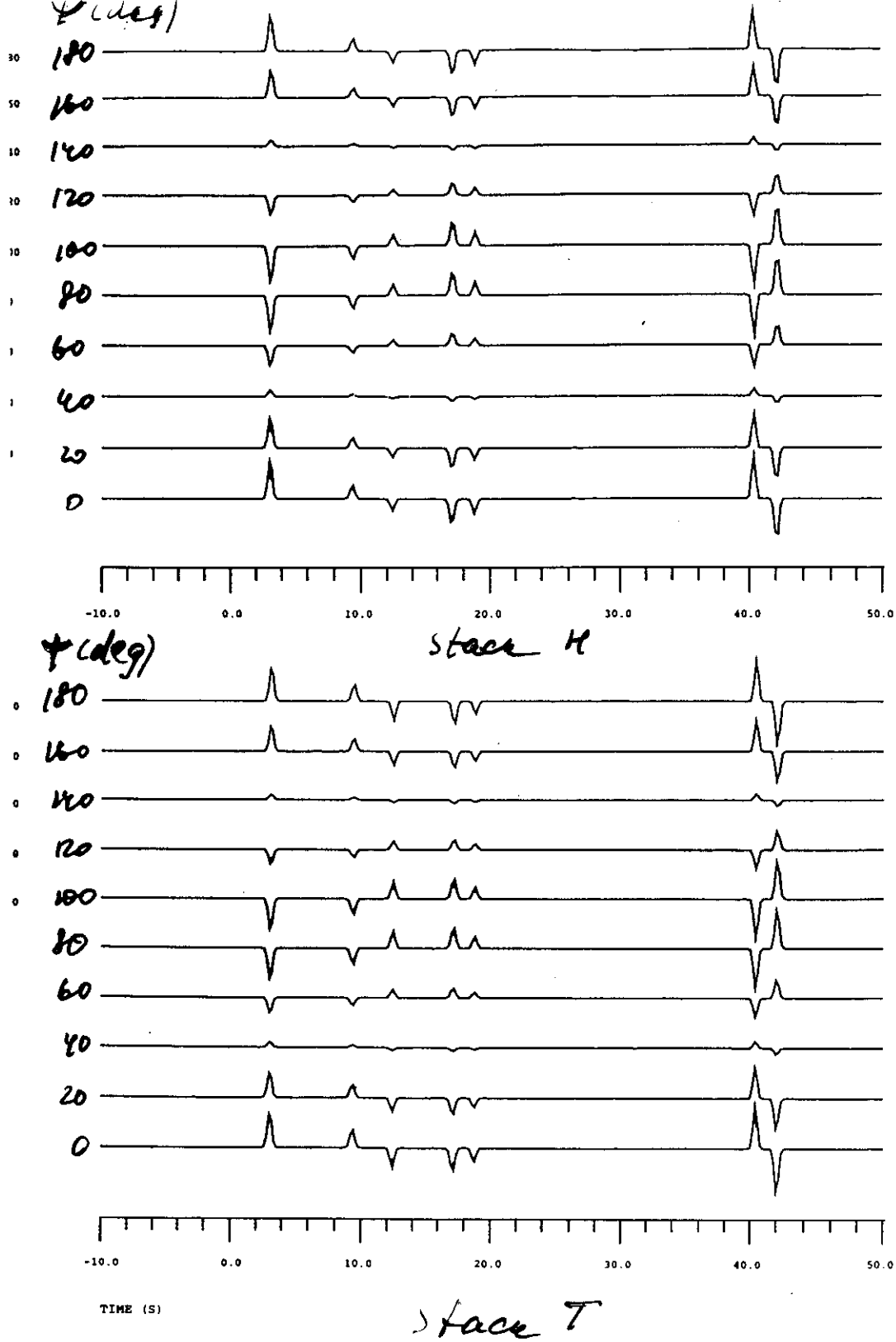
φ (deg)
180
160
140
120
100
80
60
40
20
0
-10.0
0.0
10.0
20.0
30.0
40.0
50.0
Stack H
φ (deg)
180
160
140
120
100
80
60
40
20
0
-10.0
0.0
10.0
20.0
30.0
40.0
50.0
TIME (S)
Stack T

Figure 7